Astronomy & Astrophysics

The VIMOS Public Extragalactic Redshift Survey

Measuring the growth rate of structure around cosmic voids[*]

A. J. Hawken[1], B. R. Granett[1], A. Iovino[1], L. Guzzo[1, 2], J. A. Peacock[12], S. de la Torre[4], B. Garilli[3], M. Bolzonella[8],
M. Scodeggio[3], U. Abbas[5], C. Adami[4], D. Bottini[3], A. Cappi[8, 17], O. Cucciati[15, 8], I. Davidzon[4, 8], A. Fritz[3],
P. Franzetti[3], J. Krywult[13], V. Le Brun[4], O. Le Fèvre[4], D. Maccagni[3], K. Małek[14, 19], F. Marulli[15, 16, 8], M. Polletta[3],
A. Pollo[18, 19], L. A. M. Tasca[4], R. Tojeiro[10], D. Vergani[20, 8], A. Zanichelli[21], S. Arnouts[6], J. Bel[7], E. Branchini[9, 22, 23],
G. De Lucia[11], O. Ilbert[4], L. Moscardini[15, 16, 8], and W. J. Percival[10]

(Affiliations can be found after the references)

ABSTRACT

We aim to develop a novel methodology for measuring the growth rate of structure around cosmic voids. We identified voids in the completed VIMOS Public Extragalactic Redshift Survey (VIPERS), using an algorithm based on searching for empty spheres. We measured the cross-correlation between the centres of voids and the complete galaxy catalogue. The cross-correlation function exhibits a clear anisotropy in both VIPERS fields (W1 and W4), which is characteristic of linear redshift space distortions. By measuring the projected cross-correlation and then de-projecting it we are able to estimate the un-distorted cross-correlation function. We propose that given a sufficiently well-measured cross-correlation function one should be able to measure the linear growth rate of structure by applying a simple linear Gaussian streaming model for the redshift space distortions (RSD). Our study of voids in 306 mock galaxy catalogues mimicking the VIPERS fields suggests that VIPERS is capable of measuring β, the ratio of the linear growth rate to the bias, with an error of around 25%. Applying our method to the VIPERS data, we find a value for the redshift space distortion parameter, $\beta = 0.423^{+0.104}_{-0.108}$ which, given the bias of the galaxy population we use, gives a linear growth rate of $f\sigma_8 = 0.296^{+0.075}_{-0.078}$ at $z = 0.727$. These results are consistent with values observed in parallel VIPERS analyses that use standard techniques.

Key words. large-scale structure of Universe – cosmology: observations – cosmological parameters – gravitation

1. Introduction

Different cosmological models, and different theories of gravity, predict that the large scale distribution of matter should be structured in subtly different ways. The light emitted from galaxies can be used as a proxy to trace this weblike structure. The cosmic web can be split into different component structures that show different properties, namely nodes (clusters), filaments, walls, and voids. Cosmic voids are the most underdense regions of the universe, and compose most of its volume (Sheth & van de Weygaert 2004). Their abundance can be used as a probe of the growth of structure (Jennings et al. 2013). They are also the most dark-energy-dominated environments and therefore are ideal places in which to study vacuum energy and to search for signatures of modified gravity (Goldberg & Vogeley 2004; Clampitt et al. 2013; Zivick et al. 2015; Cai et al. 2015).

There are many competing explanations for the observed accelerating expansion of the Universe. Many of these models can reproduce the same expansion history, therefore measurements of the expansion history alone, either using standard candles like type 1a supernovae, or standard rulers such as baryon acoustic oscillations, cannot discriminate between them. However, theories that modify general relativity or the equation of state of dark energy may alter the effective strength of gravity and thus also the growth rate of structure. Therefore, measuring the growth rate of structure at different redshifts is necessary to break the degeneracy between modified gravity and dark energy (Albrecht et al. 2009).

Galaxies that trace cosmic structure are subject to motions in addition to the Hubble flow. These motions contribute to the observed redshift of a galaxy and distort its apparent position in space (Kaiser 1987; Hamilton 1998). Measuring the growth rate of structure is a technical challenge because even on the largest scales accessible to cosmological surveys the gravitational peculiar motions of galaxies are not fully linear. However, the density of material close to the edges of voids is of the same order of magnitude as the mean cosmic density. Therefore the relationship between density and velocity fields should be linear (Paz et al. 2013; Hamaus et al. 2014b). Here we propose a novel method that utilises the linear nature of the velocity field around cosmic voids to extract a measurement of the growth rate of structure.

A galaxy in or close to the edge of a void is probably being evacuated away from the void centre, falling onto the surrounding structure under the influence of gravity (Padilla et al. 2005; Dubinski et al. 1993). These redshift space distortions (RSD) introduce an anisotropy to the void-galaxy cross-correlation

---

function, ξ_{vg} (Paz et al. 2013; Hamaus et al. 2014a, 2015, 2016; Cai et al. 2016; Chuang et al. 2017; Achitouv & Blake 2017). If all anisotropy in the void-galaxy cross-correlation function arises via RSD, and the relationship between the velocity and density fields is understood, then the strength of the RSD signal can be measured given a model for the isotropic density field around voids.

In Sect. 2 we give an overview of the search for voids in our data set, the VIMOS Public Extragalactic Redshift Survey (VIPERS[1]). We also describe the mock catalogues used in our analysis. In Sect. 3 we describe a toy model for the void-galaxy cross-correlation function that we later use to test our methodology. We outline our model for the anisotropies caused by linear redshift space distortions in Sect. 4. Our measurements of the cross-correlation are described in Sect. 5. In Sect. 6 we describe how, by de-projecting the projected void-galaxy cross-correlation function, we can estimate the realspace void density profiles. We describe how we built covariance matrices from the mock catalogues and fitted our model to the mocks in Sect. 7, and in Sect. 8 we describe how we fitted our model to the data. By doing this it is possible to extract a measurement of the growth rate of structure, $f(\Omega)$. We conclude in Sect. 9, where we also discuss our results and methodology with reference to recent progress by others in this field.

2. The search for voids in the VIMOS Public Extragalactic Redshift Survey

The VIMOS Public Extragalactic Redshift Survey (VIPERS) is an ESO Large Programme, started at the end of 2008, to map in detail the spatial distribution of galaxies with magnitude $i_{AB} < 22.5$ over an unprecedented volume of the Universe up to $z \sim 1$. Its goals are to accurately and robustly measure galaxy clustering, galaxy properties, and the growth of structure at an epoch when the Universe was about half its current age. The galaxy target sample is based on five-band photometric data from the Canada-France-Hawaii Telescope Legacy Survey Wide catalogue (CFHTLS-Wide; Cuillandre et al. 2012). VIPERS is split over two CFHTLS fields named W1 and W4.

The survey is particularly narrow in declination, 1.8° in W1 and 1.6° in W4, which makes it difficult to use common void-finding techniques such as the watershed algorithm (Platen et al. 2007; Neyrinck 2008; Sutter et al. 2012). Furthermore, many watershed void-finders discard voids that intersect the survey boundaries. Most visible underdensities in VIPERS intersect with the survey boundaries due to the geometry of the survey and are therefore excluded by these algorithms. We therefore developed an algorithm that searches for voids using empty spheres, which is described in detail in Micheletti et al. (2014).

Following Micheletti et al. (2014) we searched for voids in a volume-limited sample of galaxies from the VIPERS final data release with a redshift $0.55 < z < 0.9$, selecting galaxies with an absolute magnitude $M_B - 5\log h < -19.3 - z$, that have spectroscopic flags ≥ 2, meaning those have redshifts measured using two or more spectral lines (for a full explanation of VIPERS spectroscopic flags please see Garilli et al. 2014). This corresponds to regions approximately $695\,h^{-1}$ Mpc long, and 58 by $265\,h^{-1}$ Mpc in W1, and 51 by $168\,h^{-1}$ Mpc in W4, at a redshift of $z = 0.75$. The total volume in which we searched for voids was then approximately $1.6 \times 10^7\,(h^{-1}\,\text{Mpc})^3$. Our volume limited catalogue for W1 contains 23210 objects and for W4 contains 11426 objects. We then grew empty spheres on a fine regular
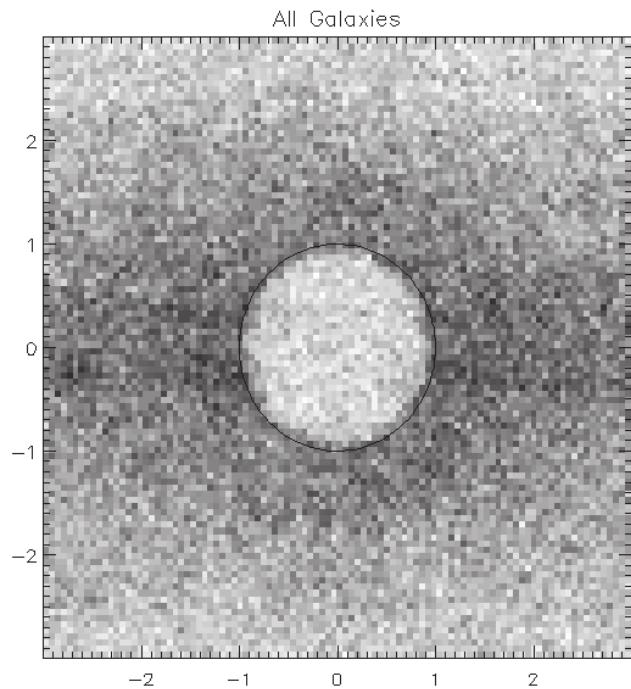
Fig. 1. Stacked voids in VIPERS PDR-2. This figure shows the density of galaxies in PDR-2 relative to the centres of voids. The $x - y$ plane of the figure corresponds to the plane of the sky in comoving coordinates, rescaled to the radii of the voids. The black circle indicates $r/r_s = 1$, i.e. the normalised radius of the stacked voids. The thickness of each slice in the stack is 0.25 void radii.

grid of resolution $0.7\,h^{-1}$ Mpc. The radius of the largest empty sphere centred on each grid point was simply the distance to the nearest galaxy. The VIMOS mask leaves gaps corresponding to $\sim 1-2\,h^{-1}$ Mpc, to avoid selecting spurious underdensities that are generated by masking effects we limited ourselves to only searching for the most significant empty spheres. In practice this meant that the empty spheres we were interested in have a radius $\gtrsim 8\,h^{-1}$ Mpc. This is smaller than the minimum radius in Micheletti et al. (2014), which was defined in a different way and was overly conservative. Spheres were discarded if more than 20% of their volume lay outside the survey boundaries. We defined voids as being statistically significant spheres that do not overlap. We identified 822 voids in the W1 field of VIPERS, and 441 voids in W4.

Figure 1 shows all the voids in the two fields stacked on top of one another. The $x - y$ plane of Fig. 1 corresponds to the plane of the sky in co-moving coordinates, re-scaled to the radii of the voids. The thickness of each slice in the stack is 0.25 void radii. The points represent the density of galaxy positions, which have been re-scaled by the radii of the spheres. One can see that on average these under densities are spherically symmetric with an apparent over-dense ridge between one and two void radii from the centre. One can also see that there is an enhancement in the apparent density of galaxies along the x axis, which is a systematic effect due to the geometry of VIPERS. The two fields are broad in right ascension and narrow in declination. This has the effect that galaxies are more likely to be found to the left or right of voids on the plane of the sky than above or below. Systematic effects such as this, caused by the geometry of the survey, are the primary reason why the stacked density profile is not as useful a measurement as the void-galaxy cross-correlation function.
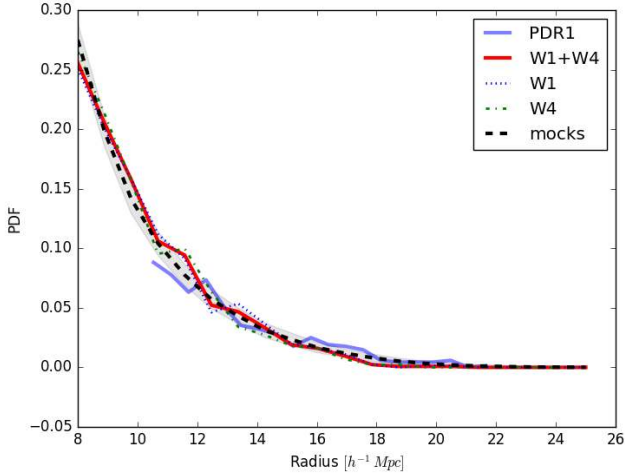
Fig. 2. Normalised histogram of void radii in this data set (red solid line) compared to those in the mock catalogues (black dashed line). The grey band shows the standard deviation of the void size histogram in the mocks. The blue and green dotted lines show the two individual fields in this data set. The histogram of void sizes in Micheletti et al. (2014) is also plotted (blue solid line). We note that this has been renormalised to account for the change in minimum void radius is this work.

There is a notable increase in sky coverage, mainly in W1, in PDR-2 compared to the first public data release, PDR-1. Additionally, pointings within the survey borders that were missing in PDR-1 have since been re-observed. This has had an effect on the apparent size and distribution of voids near these regions. Although there is not a one-to-one correspondence between voids in the current data set and those in PDR-1, in general the properties of the voids in the new catalogue are not appreciably different from those presented in Micheletti et al. (2014). Figure 2 shows the normalised histogram of void radii in this data set compared to the mock catalogues (see Sect. 2.1 for a description of the mocks). The distribution of sizes is consistent with the mock catalogues and PDR-1. There are no suspicious differences between the two fields.

2.1. Mock galaxy catalogues

The mock galaxy catalogues that we used were constructed by populating a large N-body simulation with galaxies using a halo occupation distribution (HOD). The haloes were taken from the dark matter halo catalogue of the BigMultiDark simulation (Prada et al. 2012). This simulation has a Λ-CDM cosmology, in which $\Omega_m = 0.31$, $\Omega_\Lambda = 0.69$, $\Omega_b = 0.048$, $\sigma_8 = 0.82$, $n_s = 0.96$, and $h = 0.7$. The original halo catalogue is limited in mass to haloes below $\sim 10^{12}\,M_\odot\,h^{-1}$ due to the mass resolution of the simulation. To produce mock galaxies as faint as those in VIPERS the simulation was first re-populated with haloes of masses below the resolution limit by reconstructing the density field from the dark matter field, following the method described in de la Torre & Peacock (2013). The haloes were then populated using the HOD, for which the redshift evolution was calibrated using clustering measurements from VIPERS. A full description of method and parameters can be found in de la Torre et al. (2013), and in the parallel paper de la Torre et al. (in prep.).

Mocks were then extracted from the catalogue, using a VIPERS-like colour selection and magnitude limit, $i_{AB} < 22.5$. The selection function, $n(z)$, in these parent mocks was then explicitly matched to the observed redshift distribution of galaxies in the two VIPERS fields combined. Gaussian errors on redshifts were then applied, $\sigma_v = 135\,km\,s^{-1}$, corresponding to the value estimated in PDR-1. Spectroscopic masks were built for each mock using the slit positioning software, SSPOC (Bottini et al. 2004). The target sampling rate (TSR), introduced by SSPOC, is a function of the local surface density of galaxies. Thus the TSR values of the mocks differ slightly from those in the real data.

Furthermore, not all measurements of spectra using VIMOS are successful, so the spectroscopic success rate (SSR) varies from quadrant to quadrant. The SSR depends on a number of factors such as the seeing on the night the observations were taken, distance of the pointing from the ecliptic plane, and the magnitude of the source. To account for this we have randomly downsampled the mocks to have the same density as the VIPERS data.

3. Modelling the void-galaxy cross-correlation function

In this section we describe a simple model for the void-galaxy cross-correlation function, ξ_{vg}. The integrated density contrast in a void-centred sphere of radius, r, and volume, V, is

$$\Delta(r) = \frac{1}{V} \int_V \left(\frac{\rho_g(r)}{\bar{\rho}_g} - 1 \right) dV, \tag{1}$$

where $\rho_g(r)$ is the density of galaxies as a function of radius and $\bar{\rho}$ is the mean galaxy density of the universe. The void galaxy cross-correlation function is defined as

$$\xi_{vg}(r) = \frac{\rho_g(r)}{\bar{\rho}_g} - 1, \tag{2}$$

$$= \delta_g(r), \tag{3}$$

where r is the distance from the void centre (Peebles 1980). Thus the void-galaxy cross-correlation function can be expressed in terms of the integrated void density profile,

$$\xi_{vg}(r) = \frac{1}{3r^2} \frac{d}{dr} (r^3 \Delta(r)). \tag{4}$$

There are several proposed functional forms for the void density profile in the literature. These can broadly be divided into two categories: phenomenological models that seek to fit the functional form of the void density profile (e.g. Hamaus et al. 2014b; Paz et al. 2013; Nadathur et al. 2015), and theoretically motivated models (e.g. Finelli et al. 2016). Some of these models include a free parameter that allows for an over-compensating ridge around the void. Objects with ridges such as this tend to be smaller voids embedded inside overdensities and are contracting, being crushed by the surrounding overdensity (Sheth & van de Weygaert 2004). Velocities in the vicinity of these kinds of objects may be far from linear.

Sheth & van de Weygaert (2004) first observed that voids can be divided into two populations based on environment. Void-in-void objects are embedded in under-dense regions. These voids tend to be larger, and behave in a very linear way, expanding as structure in the Universe grows. The density profiles of these voids typically asymptote to the mean density of the Universe with little or no compensating ridge around them. Void-in-cloud objects are voids that are embedded in over-dense regions. These voids typically have heavily over-compensated density profiles and their dynamical properties are less linear. Furthermore, they typically shrink as structure grows, becoming

crushed by the surrounding overdensity. However, the interiors are still being evacuated and their immediate surroundings are still expected to be linear.

Here we propose a simple stretched exponential form for the integrated density contrast of galaxies,

$$\Delta(r) = \delta_c \exp\left(-\left(\frac{r}{r_v}\right)^\alpha\right). \tag{5}$$

This model has three parameters: the central density of the void, δ_c; some scale radius, r_v; and the shape parameter, α. The correlation function for this profile is easy to write analytically:

$$\xi_{vg}(r) = \delta_c \left(1 - \frac{\alpha}{3}\left(\frac{r}{r_v}\right)^\alpha\right)\exp\left(-\left(\frac{r}{r_v}\right)^\alpha\right). \tag{6}$$

This simple functional form is plotted in Fig. 3. It is interesting to note that a Gaussian profile is a special case of this model, where $\alpha = 2$. We use this model density profile to test our method for measuring the growth rate in Sect. 7.3, but in this paper we do not fit it to the observed density profile.

4. Linear redshift space distortion model

In this section we describe our linear model for the redshift space distortions around voids. The line-of-sight pairwise velocity distribution can generally be described using the streaming model, so the anisotropic void-galaxy cross-correlation function can be written:

$$1 + \xi_{vg}(r_\parallel, r_\perp) = \int_{-\infty}^{+\infty} \frac{dw_3}{\sqrt{2\pi}\sigma_v(r)}$$
$$\times \exp\left(-\frac{(w_3 - v(r)r_3/r)^2}{2\sigma_v^2(r)}\right)[1 + \xi_{vg}(r)], \tag{7}$$

where $r_3 = r_\parallel - w_3/H_0$, $r^2 = r_\perp^2 + r_3^2$, and w_3 is the line of sight component of the pairwise velocity.

The velocity dispersion of galaxies, $\sigma_v(r)$, is a function of distance from the void centre and has units of km s^{-1} h^{-1} Mpc, in other words velocity per void radius. Multiple studies have shown that $\sigma_v(r)$ is strongly scale-dependent within and around the void radius (Hamaus et al. 2015; Cai et al. 2016). However, in our analysis we assume it is constant.

A known and quantifiable source of apparent dispersion in the streaming velocity of galaxies is the error on the redshift measurement. In our mock galaxy catalogues a Gaussian error of $\sigma_z = 135$ km s^{-1} was applied. This is somewhat small compared to the estimated error in this data set, $\sigma_z = 140$ km s^{-1}. By weighting using the distribution of void sizes we were able to estimate the effective contribution to σ_z,

$$\sigma_v = \sum_i \frac{\sigma_z}{r_s^i} w_i, \tag{8}$$

where r_s^i is the radius of voids in bin i and w_i is the weight of that bin. The weights were determined using the histogram of void sizes (see Fig. 2), normalised such that $\sum_i w_i = 1$. For the mocks the effective dispersion is $\sigma_v = 13.4$ km s^{-1} (h^{-1} Mpc)$^{-1}$, and for the data this is $\sigma_v = 13.8$ km s^{-1} (h^{-1} Mpc)$^{-1}$.

Because the densities involved are very low, the gravitational dynamics of galaxies around voids, particularly larger ones, remain in the linear regime (Cai et al. 2016). This should be particularly true for our void sample because our voids are relatively large and so are expected to be more linear. Close to the centres of voids $\delta \sim -1$, therefore the relationship between the density
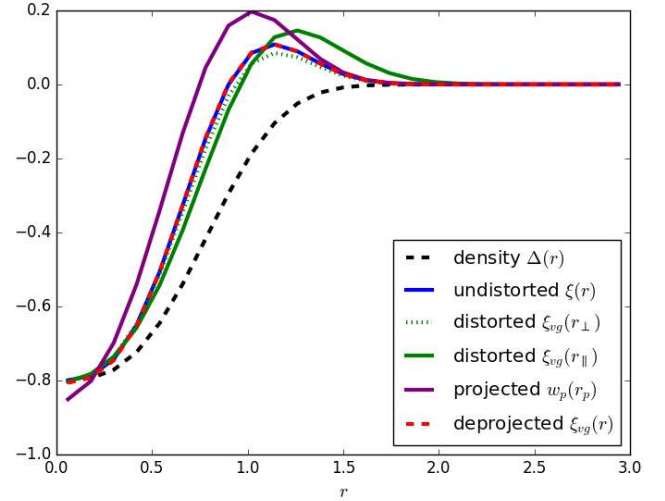
Fig. 3. Model for the void-galaxy cross-correlation function. The integrated density contrast, Eq. (5), is plotted as a black dashed line. The one dimensional void-galaxy cross-correlation function, without redshift space distortions, is plotted as a solid blue line. The void-galaxy cross-correlation function with redshift space distortions, as seen directly along the line of sight, is plotted as a solid green line. The dotted green line is the same model as seen tangential to the line of sight. The projected cross-correlation function is plotted as a purple line. The deprojection is plotted as a red dashed line, it matches the blue line very closely. The values of the model parameters are $\beta = 0.8, \sigma_v = 13.4$ km s^{-1} (h^{-1} Mpc)$^{-1}, \delta_c = -0.8, r_v = 0.9, \alpha = 3.0$.

and velocity fields is not strictly speaking linear. However, because these regions are very sparsely populated by tracers they do not contribute much to the overall signal and so their non-linear contributions can be ignored. We therefore make the assumption that the linear estimate for the relationship between the density and velocity fields remains valid, and that the relationship between the velocities of galaxies and that of matter is unbiased (Peebles 1980),

$$v(r) = -\frac{H(z)}{1+z} r\Delta(r) \frac{\beta}{3}, \tag{9}$$

where $\beta = f(z)/b$ is the redshift space distortion parameter, b is the galaxy bias, and $f(z)$ is the linear growth rate parameter, defined as the logarithmic derivative of the linear growth factor, $D(a)$, with respect to the scale factor, $f = d\ln D/d\ln a$. The growth factor is commonly parameterised as $f(z) = \Omega_m^\gamma(z)$, which is useful because it gives an approximate solution to the growth equation for a wide variety of gravity models (Peebles 1980; Wang & Steinhardt 1998; Linder 2005; Linder & Cahn 2007). In standard general relativity $\gamma \sim 0.55$. Any deviation from this value could be taken as evidence in favour of modifying general relativity. It could point to the accelerated expansion of the universe being driven by a dark energy that cannot be modelled as a cosmological constant.

A correct description of the velocity field should also consider the impact of galaxy biasing. It is well known that galaxies inhabiting voids have notably different properties from galaxies outside of voids, and in fact this is the subject of many void studies. These studies have established that galaxies inhabiting voids are typically bluer, of later type, and with higher specific star formation rate than other field galaxies (Rojas et al. 2004; Patiri et al. 2006; von Benda-Beckmann & Mueller 2007; Hoyle et al. 2012; Kreckel et al. 2012; Ricciardelli et al. 2014).

Thus one should expect that the galaxy bias in this case is heavily scale-dependent. Models have been proposed to describe how haloes are biased as a function of distance from the void centre (Neyrinck et al. 2014), therefore extending the model to include a scale-dependent bias would certainly be possible. However, for now, we consider the bias to be constant. We also make the assumption that the Hubble expansion rate and the angular diameter distance are well-constrained and therefore we neglect any potential geometric distortions due to the Alcock-Paczynski effect.

5. Measuring the void-galaxy cross-correlation function

In this section we describe our estimator for the void-galaxy cross-correlation function, ξ_{vg}. The estimated value of ξ_{vg}, in a bin of separation ij, is equal to the estimated overdensity in that bin,

$$\hat{\xi}_{vg}(r_{\parallel}^i, r_{\perp}^j) = \hat{\delta}_g^{ij} \tag{10}$$

$$= \frac{n_g^{ij}}{f^{ij}\bar{n}_g} - 1, \tag{11}$$

where $\bar{n}_g$ is the mean number density of galaxies per bin, n_g^{ij} is the number of galaxies counted in bin ij, and f^{ij} is the fraction of the bin which is unmasked, meaning that which lies completely within the survey boundaries. The fraction f^{ij} is estimated using a random catalogue with the same angular and redshift selection function as the galaxies, $f^{ij} = n_r^{ij}/\bar{n}_r$, where n_r^{ij} is the number of random points counted in the bin and $\bar{n}_r$ is the mean number density of random points. The estimator of the cross-correlation can then be written

$$\hat{\xi}_{vg}(r_{\parallel}^i, r_{\perp}^j) = \frac{n_g^{ij}}{n_r^{ij}}\frac{N_r}{N_g} - 1, \tag{12}$$

where N_r is the total number of random points and N_g is the total number of galaxies. This is simply the Davis and Peebles estimator for the cross-correlation (Davis & Peebles 1983).

As mentioned above, random catalogues were constructed in such a way as to have the same angular and radial selection functions as the data. We did this by applying the same photometric masks to initially uniform distributions of random points covering the two fields. Redshifts were then assigned to the random points by sampling from the redshift distribution of mock galaxies.

The cross-correlation function presented here is the cross-correlation between the centres of the voids and the full VIPERS PDR-2 galaxy catalogue. Void-galaxy pair separations are scaled in units of the radius of the maximal spheres, r_s, so that $\xi_{vg}(\tilde{r}_{\parallel}, \tilde{r}_{\perp}) = \xi_{vg}(r_{\parallel}/r_s, r_{\perp}/r_s)$.

Figure 4 shows ξ_{vg} measured in 10×10 bins individually in the two separate VIPERS fields, and the combined measurement of the full sample (see Sect. 6 for a discussion on selecting the number of bins). The enhancement of the correlation function along the line of sight is clearly visible. The measurement in the W4 field appears to be noisier than W1, but this is to be expected because the field is smaller. For comparison we also plot the mean cross-correlation of the 306 mock catalogues.

6. De-projecting the cross-correlation

To determine the degree to which the anisotropic cross-correlation function is distorted, we must first seek to determine

what the un-distorted cross-correlation looks like. We do this by de-projecting the projected cross-correlation function (Eisenstein 2003; Ross et al. 2007; Pisani et al. 2014).

By integrating along the line-of-sight direction we can obtain a measurement of the projected void-galaxy cross-correlation function,

$$w_{vg}(r_p) = 2\int_0^{\infty} \xi_{vg}(r_{\perp}, r_{\parallel})dr_{\parallel}. \tag{13}$$

The projected cross-correlation is, in principle, unaffected by redshift space distortions. In practice, this integral does not extend to infinity but to some $r_{\parallel}^{max}$, which is constrained by the depth of the survey. Because $\xi_{vg}(r)$ is expected to be zero at large r, we truncate the integral at $r_{\parallel}^{max}/r_v = 3$. Truncating at larger distances than this simply adds noise to the measurement. The projected void-galaxy cross-correlation function can also be written as

$$w_{vg}(r_p) = 2\int_{r_p}^{\infty} \xi_{vg}(r)\frac{r\,dr}{\sqrt{r^2 - r_p^2}}. \tag{14}$$

Given that we assume the true cross-correlation function to be isotropic we can invert Eq. (14) using the Abel transform to obtain an estimate of $\xi_{vg}(r)$,

$$\xi_{vg}(r) = -\frac{1}{\pi}\int_r^{\infty}\frac{dw(r_p)}{dr_p}\frac{dr_p}{\sqrt{r_p^2 - r^2}}. \tag{15}$$

For a given bin r_i this can be calculated using

$$\xi_{vg}(r_i) = -\frac{1}{\pi}\sum_{j \geq i}\frac{w_{vg,j+1} - w_{vg,j}}{r_{p,j+1} - r_{p,j}}\ln\left(\frac{r_{p,j+1} + \sqrt{r_{p,j+1}^2 - r_i^2}}{r_{p,j} + \sqrt{r_{p,j}^2 - r_i^2}}\right), \tag{16}$$

where $w_{vg,j}$ is the value of $w_{vg}(r_{p,j})$, the projected cross-correlation function in bin $r_{p,j}$. The number of bins has an effect on the accuracy of the projection and de-projection of the correlation function. Firstly by introducing integration noise when integrating over the line of sight. Secondly because when applying the model of the RSD we linearly interpolate both $\xi(r)$ and $\Delta(r)$. Thirdly because deprojecting involves numerical differentiation. In practice we can reduce any systematic bias introduced by the numerical differentiation in Eq. (16) by interpolating between bin centres using a cubic spline.

The number of bins in which we can measure ξ_{vg} is limited not only by the amount and quality of the data but also by the number of mocks we have available to build the covariance matrices. When we measure $\xi_{vg}(r_{\parallel}, r_{\perp})$ in 25×25 bins in the data it is very noisy. However, integrating over $r_{\parallel}$ removes much this noise. Therefore we measured the projected correlation function in 25×25 bins, but when we de-project and then used the result in an anisotropic fit to $\xi_{vg}(r_{\parallel}, r_{\perp})$ we fitted to 10×10 bins (as shown in Fig. 4).

To obtain the empirical estimate of the void density profile we first combined the measured cross-correlation functions in the two fields by weighting them based on the number of voids found in that field,

$$\xi_{W1+W4} = \xi_{W1}\frac{N_{voids}^{W1}}{N_{voids}^{tot}} + \xi_{W4}\frac{N_{voids}^{W4}}{N_{voids}^{tot}}. \tag{17}$$

The de-projection procedure was then followed to build an estimate of the un-distorted ξ_{vg} based on all the available data.
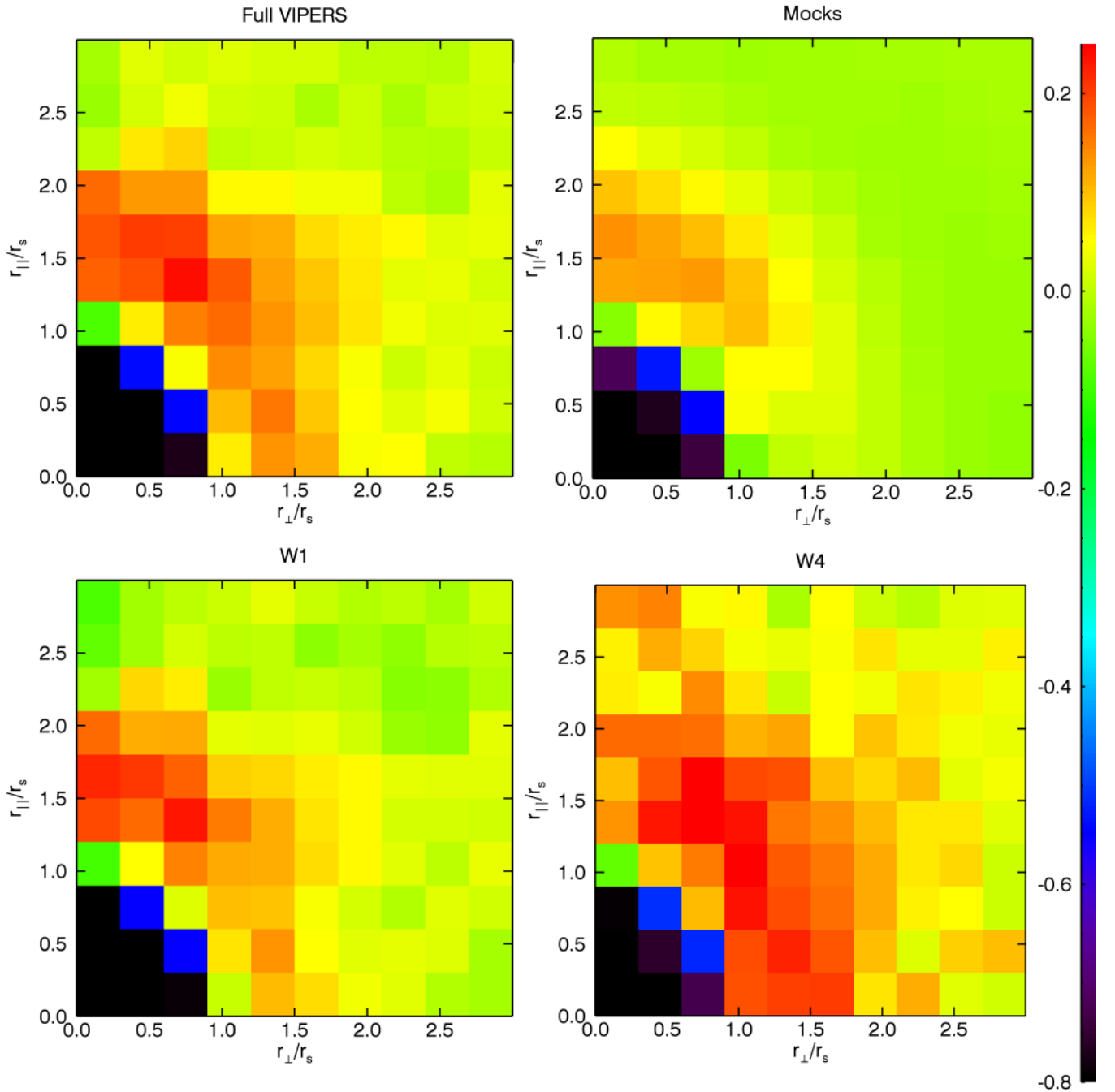
Fig. 4. Cross-correlation function between the centres of voids and the full sample of galaxies in VIPERS. The *bottom two panels* show the measured cross-correlation in the two individual VIPERS fields. The *top left panel* shows the average of these two fields. The *top right panel* shows the mean cross-correlation function of the 306 mock catalogues for comparison. The axes are in units of void radii.

Because there is no reason to believe that the density profiles of voids in the two fields would be significantly different, we applied the same model to both fields. This also allowed us to make a meaningful comparison between measurements of the growth rate from the two fields.

7. Measuring the growth rate

In this section we describe our method for constraining the growth rate of structure by fitting the model outlined in Sect. 4

to the measurement of the void-galaxy cross-correlation function, $\xi_{vg}(r_\parallel, r_\perp)$, presented in Sect. 5.

We measured ξ_{vg} in 306 mock galaxy catalogues covering W1 and W4. From these measurements we constructed covariance matrices for each field, Sect. 7.1. The input cosmology of the mocks was known, and thus so was the linear growth rate $f(z)$. However, our method provided us with an estimate of $\beta = f/b$, and so to confirm that we were able to constrain the growth rate correctly we had to first measure the bias of the galaxies we were using in the mocks, Sect. 7.2. Once the correct

growth rate was extracted from the mocks, Sect. 7.4, and any systematic bias in the measurement quantified, we placed a constraint on the growth rate in the data using the variance of recovered values from the mocks as our error bar, Sect. 8.

7.1. Covariance matrix and likelihood estimation

We ran our void-finding algorithm on each of the mocks and measured the void-galaxy cross-correlation function $\xi_{\rm vg}$ to construct a covariance matrix. There is a strong covariance between bins, this makes the covariance matrix highly non-diagonal. Thus it is important that the full covariance matrix is used to constrain the parameters of the model and not just the variance of the individual bins.

An important point to note is that in this experiment $\xi_{\rm vg}^{\rm model}$ is built using the observed cross-correlation, $\xi_{\rm vg}^{\rm obs}$, and is therefore not independent of the data. Noise present in the observations propagates through to noise in the model. Failing to account for this propagation of noise leads to a biased estimate of the growth rate and an over-estimation of the error. However, if we take care to use the correct covariance matrix and to apply the appropriate Bayesian correction factors to it then we can mitigate any introduced biases to recover the correct parameter values and their uncertainty.

The matrix $\boldsymbol{\Delta}$ is defined as the difference between the observed anisotropic void-galaxy cross-correlation function and the reprojected cross-correlation given a model for the RSD,

$$\Delta_i = \xi_{\rm vg}^{\rm obs}(r_\parallel, r_\perp)_i - \xi_{\rm vg}^{\rm model}(r_\parallel, r_\perp)_i, \tag{18}$$

where i indicates the bin in $r_\parallel$ and $r_\perp$. The mean residual between the model, given the fiducial cosmology, and $\xi_{\rm vg}(r_\parallel, r_\perp)$ observed in the mocks is

$$\mu_i = \frac{1}{N_{\rm mocks}} \sum_{k=1}^{N_{\rm mocks}} \Delta_i^k. \tag{19}$$

This quantifies the extent to which the model is biased. The expectation value of the data does not correspond to the model and therefore $\mu \neq 0$. This is because our model for the RSD is an imperfect description of the anisotropy, therefore even if the cosmology is known then the exact anisotropic cross-correlation cannot be completely recovered. One consequence of this is that the expectation value of the data matrix is not equal to the true covariance matrix, meaning that $\langle \boldsymbol{\Delta\Delta} \rangle \neq \boldsymbol{C}$. The correct covariance matrix in this instance can be defined as the expectation of the difference between the model and the observations minus the mean residual,

$$C_{ij} = \frac{1}{N_{\rm mock} - 1} \sum_{k=1}^{N_{\rm mock}} (\Delta_i^k - \mu_i)(\Delta_j^k - \mu_j). \tag{20}$$

The likelihood of a set of parameter values, $\boldsymbol{\theta}$, given the observation is then,

$$\mathcal{L}(\boldsymbol{\theta}) = \exp\left(\frac{-\chi^2}{2}\right), \tag{21}$$

where

$$\chi^2 = (\boldsymbol{\Delta} - \boldsymbol{\mu})^T \boldsymbol{C} (\boldsymbol{\Delta} - \boldsymbol{\mu}), \tag{22}$$

with $\boldsymbol{\mu}$ being the residual matrix as measured in the mocks, given by Eq. (19). This assumes that the likelihood $\mathcal{L}(\boldsymbol{\theta})$ is Gaussian, which we do not know to be true. We can test the Gaussianity of

the likelihood by looking at the scatter of recovered values from mock catalogues (see Sect. 7.4). The covariance matrices are calculated individually for each field. The combined likelihood for the full survey is calculated by summing the χ^2 for each field:

$$\chi^2_{W1+W4} = (\boldsymbol{\Delta}_{W1} - \boldsymbol{\mu})^T \boldsymbol{C}_{W1}(\boldsymbol{\Delta}_{W1} - \boldsymbol{\mu}) + (\boldsymbol{\Delta}_{W4} - \boldsymbol{\mu})^T \boldsymbol{C}_{W4}(\boldsymbol{\Delta}_{W4} - \boldsymbol{\mu}). \tag{23}$$

The covariance matrix defined in Eq. (20) is biased because the number of mocks used to produce it is finite, and of the same order as the number of degrees of freedom. The bias of this estimate can be corrected for by replacing it in the likelihood calculation with a matrix $\boldsymbol{\Psi}$ defined as (Hartlap et al. 2007)

$$\boldsymbol{\Psi} = (1 - \mathcal{D})\boldsymbol{C}^{-1}, \tag{24}$$

where

$$\mathcal{D} = \frac{N_{\rm bins} + 1}{N_{\rm mocks} - 1}. \tag{25}$$

We note that we do not incorporate the remaining statistical uncertainty in $\boldsymbol{C}$ into our likelihood, although in principle this can be done (Sellentin & Heavens 2016).

The mock catalogues were built using an HOD which was constructed so that the projected two-point clustering of galaxies matched observations. They were not constructed with an analysis of void properties in mind. Furthermore, regions corresponding to $W1$ and $W4$ were sometimes cut from the same simulation boxes. Additionally, the bias and colour evolution of galaxies in the mocks are not completely accurate. These effects can lead to inaccuracies of our covariance matrix. These errors in the covariance matrix should be propagated correctly.

We wanted to determine the combined error on the measurement, including both the uncertainties inherent in the data and the noisy covariance matrix. To obtain an unbiased estimate of the full error we had to also multiply the inverse covariance matrix by a factor of m_1 (Percival et al. 2014),

$$m_1 = \frac{1 + B(N_{\rm bins} - N_{\rm p})}{1 + A + B(N_{\rm p} + 1)}, \tag{26}$$

where $N_{\rm p}$ is the number of parameters in the model, and where

$$A = \frac{2}{(N_{\rm mocks} - N_{\rm bins} - 1)(N_{\rm mocks} - N_{\rm bins} - 4)}, \tag{27}$$

$$B = \frac{N_{\rm mocks} - N_{\rm bins} - 2}{(N_{\rm mocks} - N_{\rm bins} - 1)(N_{\rm mocks} - N_{\rm bins} - 4)}. \tag{28}$$

An accurate estimate of the uncertainty on the growth rate measured from VIPERS data using our method comes from the variance of the value of β recovered from individual VIPERS-like mocks multiplied by an additional factor, m_2,

$$\sigma_\beta^{\rm data} = \sqrt{m_2}\,\sigma_\beta^{\rm mocks}, \tag{29}$$

where

$$m_2 = \frac{m_1}{1 - \mathcal{D}}. \tag{30}$$

This additional factor accounts for the fact the mocks used to test the covariance matrix were also used to construct it. The VIPERS data is completely independent of the covariance matrix and thus is biased in a different way to the mocks.

7.2. Measuring the bias

To recover the growth rate corresponding to the input cosmology from the mocks, we must first estimate the effective linear bias of mock galaxies used to measure the void-galaxy cross-correlation function. Because we knew the real space positions of galaxies in our mock catalogues, we measured the bias by taking the ratio of the real space correlation function of galaxies, $\xi_g(r)$, to the dark matter correlation function, $\xi_{dm}(r)$,

$$b^2 = \frac{\xi_g(r)}{\xi_{dm}(r)}. \tag{31}$$

Here $\xi_{dm}(r)$ is the usual dark matter two-point autocorrelation function,

$$\xi(r) = \frac{1}{(2\pi)^3} \int P_{dm}(k) \frac{\sin(kr)}{kr} 4\pi k^2 dk. \tag{32}$$

This was calculated by performing a Fourier transform of the theoretical dark matter power spectrum, $P_{dm}(k)$, generated using CAMB (Lewis & Bridle 2002). The power spectrum has the same cosmological parameters as the mocks and was calculated at the median redshift of void-galaxy pairs, which is $z = 0.727$ (see Sect. 8.1). The non-linear component of the matter power spectrum was estimated using HALOFIT (Takahashi et al. 2012). Having access to the real space positions of the mock galaxies, we measured the real space correlation function in the mocks using the Landy-Szalay estimator (Landy & Szalay 1993),

$$\xi_g(r) = \frac{DD(r) - 2DR(r) + RR(r)}{RR(r)}, \tag{33}$$

where $DD(r)$ is the number of galaxy-galaxy pairs in a given bin of co-moving separation, r, $DR(r)$ is the number of galaxy-random pairs, and $RR(r)$ is the number of random-random pairs. The bias measured in the mock catalogues is plotted in Fig. 5. The bias has some scale-dependance and therefore we take an average value. The mean bias in the mocks over the scales $5.0 \leq r_p \leq 30.0$ and its error are $b = 1.29 \pm 0.02$. The mean error for one mock is 0.05.

7.3. Testing on the toy model

We first tested the method on the toy model for the density profile presented in Sect. 3. We wanted to ensure that our method of de-projecting the cross-correlation function to estimate the void density profile did not introduce a bias on the measured growth rate. By applying our RSD model, we generated an anisotropic cross-correlation function from the toy model, with a known value of $\beta = 0.64$ and fixing $\sigma_v = 13.4$. We then treated this in the same way we would treat data. We calculated the toy model in 25×25 bins and then de-projected it to obtain an estimate of the input model density profile. This was then re-anisotropised for different values of β and σ_v, exploring the parameter space using a Markov chain Monte Carlo (MCMC) algorithm. We find that reducing the number of bins from which the de-projected cross-correlation is measured can bias the results. The true value of β is well recovered, with minimal bias being introduced by the method.

7.4. Recovering the input cosmology from the mocks

To demonstrate that the model presented in Sect. 4 is a sufficient description of the anisotropic void-galaxy cross-correlation function, we must show that we are able to extract the correct
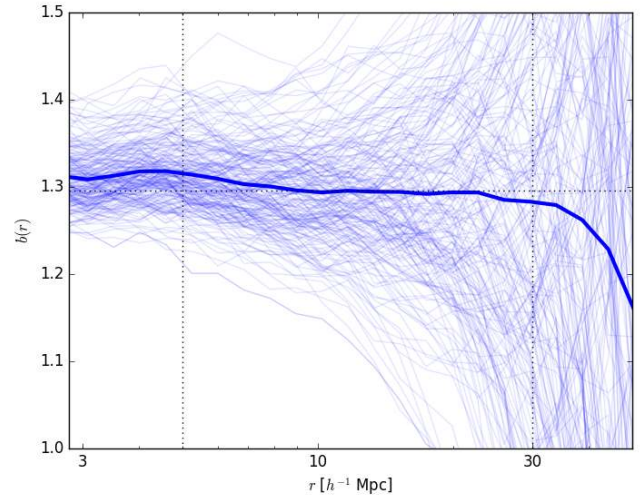

Fig. 5. Bias of mock galaxy catalogues. The faint blue lines represent the measured bias of individual mocks, the thick blue line is the mean of the mocks. Our quoted value for the mean bias (dotted horizontal line) is the mean value between $5.0 < r < 30\,h^{-1}$ Mpc which is the scale over which the bias shows the least scale-dependence (dotted vertical lines). The downturn at large scales is caused by the integral constraint.

growth rate of structure from the mock galaxy catalogues described in Sect. 2.1. This is a test both of our method and our RSD model.

The projected cross-correlation functions and the de-projected cross-correlation functions of all 306 mocks and the mean values (thick blue line) are plotted in Fig. 6 (left and right hand panels respectively). The values of $w_{vg}(r_p)$ and ξ_{vg}^d for the data are also plotted; these will be discussed in the next section. The mock catalogues were not constructed with a mind to accurately reproducing void properties, therefore the fact that there are some inconsistencies between mock and data void profiles is to be expected.

We then ran EMCEE, an implementation of the affine-invariant ensemble sampler for Markov chain Monte Carlo algorithm (Foreman-Mackey et al. 2013), to estimate the best-fitting values of β and σ_v in each of the 306 mock realisations. An accurate estimate of the uncertainty on the growth rate measured from VIPERS using our method comes from the distribution of the value of β recovered from individual VIPERS-like mocks. This also allows us to place a non-Gaussian error bar on our result. Figure 7 shows the scatter of recovered values of β and σ_v for the mocks. The top panel shows a histogram of the recovered values of β, and the grey band shows the expected value of β given the cosmology and bias of the mocks. The 16th and 84th percentiles are illustrated by the dotted blue lines. The true value of β lies very close to the mean of those recovered from the mocks. The distribution of recovered values is not strongly non-Gaussian.

8. Application to VIMOS Public Extragalactic Redshift Survey data

In this section we describe the application of the method tested on our mock catalogues in Sect. 7 to the final data release of VIPERS. In Sect. 8.1 describes how we estimate the redshift at which our measurement of β is made. We present our measurements of β in the data in Sect. 8.3. In Sect. 8.4 we then describe how we convert our measurement of β to a measurement
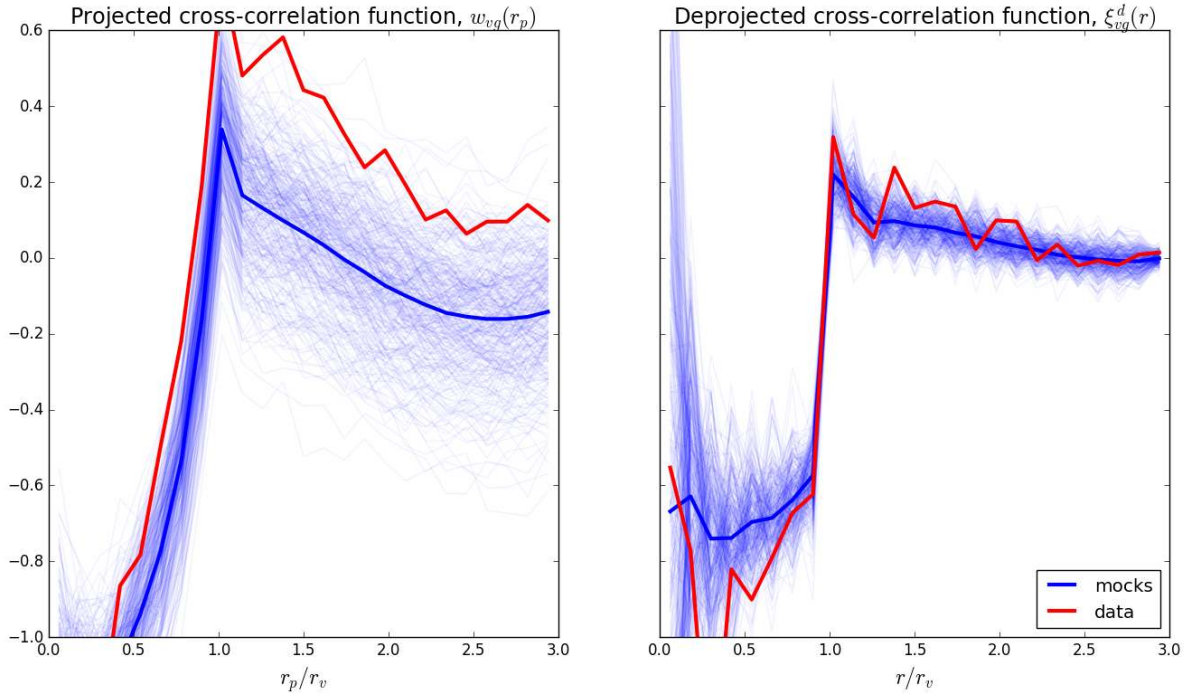
Fig. 6. Projected (*left hand panel*) and de-projected (*right hand panel*) void-galaxy cross-correlation functions for mock catalogues (blue) and the VIPERS data (red). Here the minimum void radius used is $8\,h^{-1}$ Mpc.
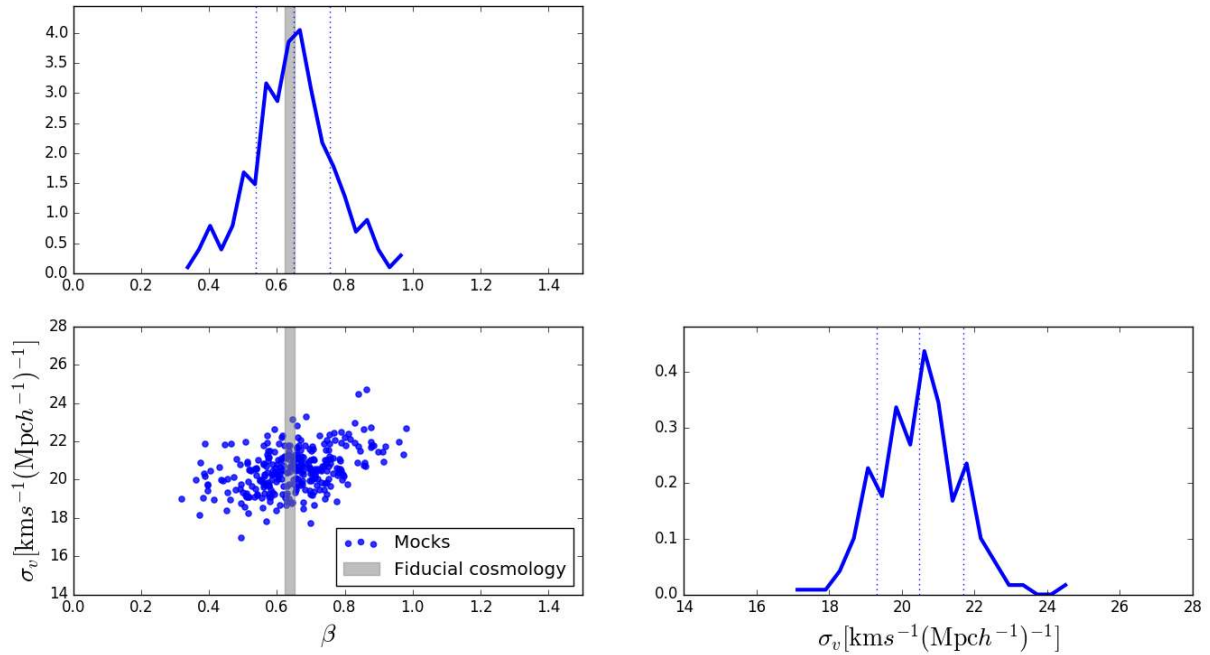

Fig. 7. Distribution of recovered values of β and σ_v from mock catalogues. Each blue point in the *bottom left panel* gives the best-fitting values of β and σ_v for the combination of two VIPERS-like mock fields. The histogram in the *top panel* shows the PDF of the recovered values of β and the *bottom right panel* gives the PDF of the recovered values of σ_v. The grey band is the expected value of β given the fiducial cosmology and the uncertainty on the bias.

of $f\sigma_8$ so that it can be compared to other measurements in the literature.

8.1. Estimating the redshift of the measurement

It is important to note that our galaxy and void samples span a considerable distance in redshift space, $0.55 < z < 0.9$. The

growth rate of structure is expected to evolve over this redshift range. The mean redshift at which we are measuring the growth rate will be a weighted combination of the radial selection functions of galaxies and voids, approximately the mean redshift of void-galaxy pairs. Figure 8 shows the normalised number of objects as a function of redshift, $N(z)$, for our void catalogue (blue line) and for the full galaxy sample (green line). The $N(z)$ of
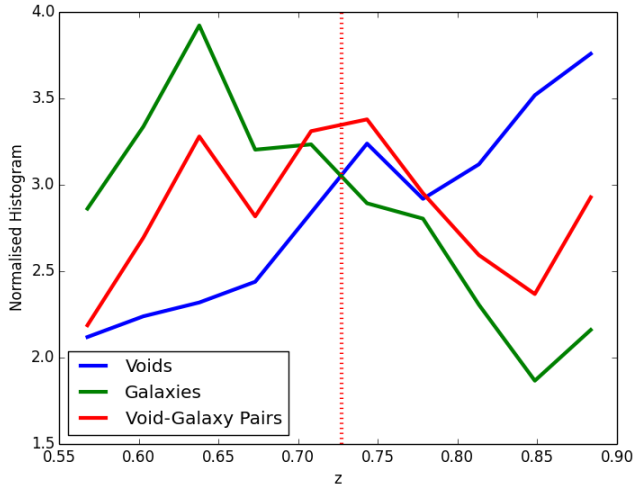
Fig. 8. Normalised number of objects as a function of redshift, $N(z)$, for voids (blue), galaxies (green), and void-galaxy pairs (red) in VIPERS. The mean redshift of void-galaxy pairs is $\bar{z} = 0.727$ (red dashed line).
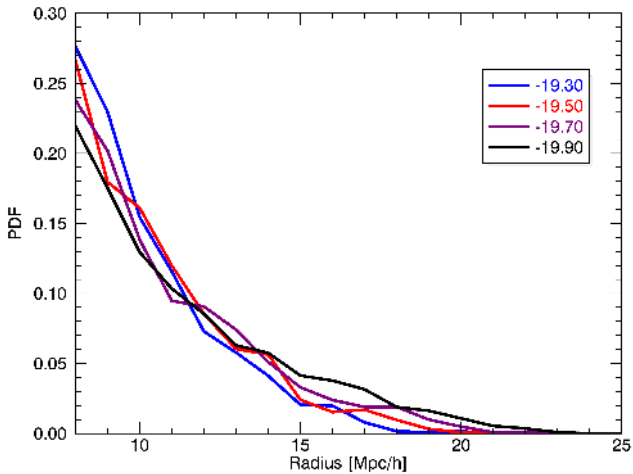

Fig. 9. Histograms showing the distribution of the size of void radii for voids found in different volume-limited catalogues.

voids rises with redshift, chiefly because there is more volume available at higher redshifts. The $N(z)$ of void-galaxy pairs is then the product of these two histograms (red line). The mean redshift of pairs, $\bar{z} = 0.727$ (red dashed line), is the redshift at which our measurement of the growth rate is made.

8.2. The effect of tracer luminosity on void properties

There are some minor differences between apparent and absolute magnitudes in different VIPERS data releases. We also know that the redshift evolution of absolute magnitudes in the mocks is not representative of the data. It is therefore useful to investigate what impact changing the magnitude limit of the volume-limited catalogue in which we search for voids could have on our measurement of the void density profile. To do this we reran our void finder on volume-limited catalogues with brighter magnitude cutoffs. Histograms showing the distribution of void radii in these samples are shown in Fig. 9. As one might expect, more luminous tracers, and thus probably more biased tracers, define larger voids. This also means that fewer voids are found in these catalogues, and thus the signal-to-noise ratio of any statistics will be reduced.

Table 1. Best-fitting parameters to the data, as estimated using an MCMC chain.

	β	σ_{v} [km s^{-1} (h^{-1} Mpc)$^{-1}$]
W1	$0.315^{+0.202}_{-0.162}$	$18.9^{+2.2}_{-2.1}$
W4	$0.505^{+0.181}_{-0.175}$	$18.8^{+2.0}_{-2.0}$
VIPERS	$0.423^{+0.134\,(+0.104)}_{-0.135\,(-0.108)}$	$19.1^{+1.6}_{-1.5}$

Notes. Errors on the estimated values are those from the MCMC. For the full VIPERS we also add errors estimated from the scatter of the mocks. The quoted errors are the 16th and 84th percentiles.

We then measured the cross-correlation between voids found in these brighter samples and the complete galaxy population (as described in Sect. 5). The corresponding projected cross-correlation functions and de-projected density profiles are plotted in Fig. 10 (left and right hand panels respectively). The larger voids defined by the brighter tracer populations have less underdense interiors. Other than that there is no clearly discernible trend. It is perhaps surprising that the brightness of the magnitude cut does not have a clear effect on the de-projected density profile.

8.3. Estimating the growth rate

Using the method described in Sect. 7 we fitted our model for the void-galaxy cross-correlation to the two VIPERS fields individually and to the combination of the two fields. Table 1 shows the best-fitting values for β and σ_{v} and their associated errors as estimated using an MCMC chain.

The uncertainties quoted in Table 1 come from the likelihood and they mis-estimate the true uncertainty in the measurement. The analysis of the mock catalogues presented in Sect. 7.4 suggests that the error bar on the total measurement should be slightly smaller, although comparable. There is no significant inconsistency between the results from the two VIPERS fields.

Figure 11 shows the contours from the MCMC analysis. It would suggest that there is a slight degeneracy between the two parameters. This degeneracy is also suggested by the scatter of best-fitting values in the mock catalogues (Fig. 7). However, given that the degeneracy is not steep, fixing σ_{v} would only have a marginal effect on the error on the measured growth rate. Nevertheless, additional prior information about the velocity dispersion of galaxies around voids would aid in further constraining the growth rate.

8.4. Comparison with other estimates of the growth rate

Conventionally, measurements of the growth rate of structure are quoted in terms of $f\sigma_8$, which is related to our measurement of β by

$$f\sigma_8 = \beta\sigma_8^{\mathrm{galaxies}}. \tag{34}$$

The values of σ_8 on the left and right hand side of the above equation are the "linear" values of σ_8 for dark matter and galaxies respectively. Thus, to compare our measurement of β in VIPERS with other growth rate measurements we had to also measure the value of σ_8 of galaxies in the data. The real space, "nonlinear", σ_8 of galaxies can be estimated from the projected galaxy autocorrelation function (Zehavi et al. 2005; Eisenstein 2003),

$$\sigma_R^2 = \frac{1}{R^3}\int_0^\infty r_{\mathrm{p}}\, w_{\mathrm{p}}(r_{\mathrm{p}})\, g(r_{\mathrm{p}}/R)\, \mathrm{d}r_{\mathrm{p}}, \tag{35}$$
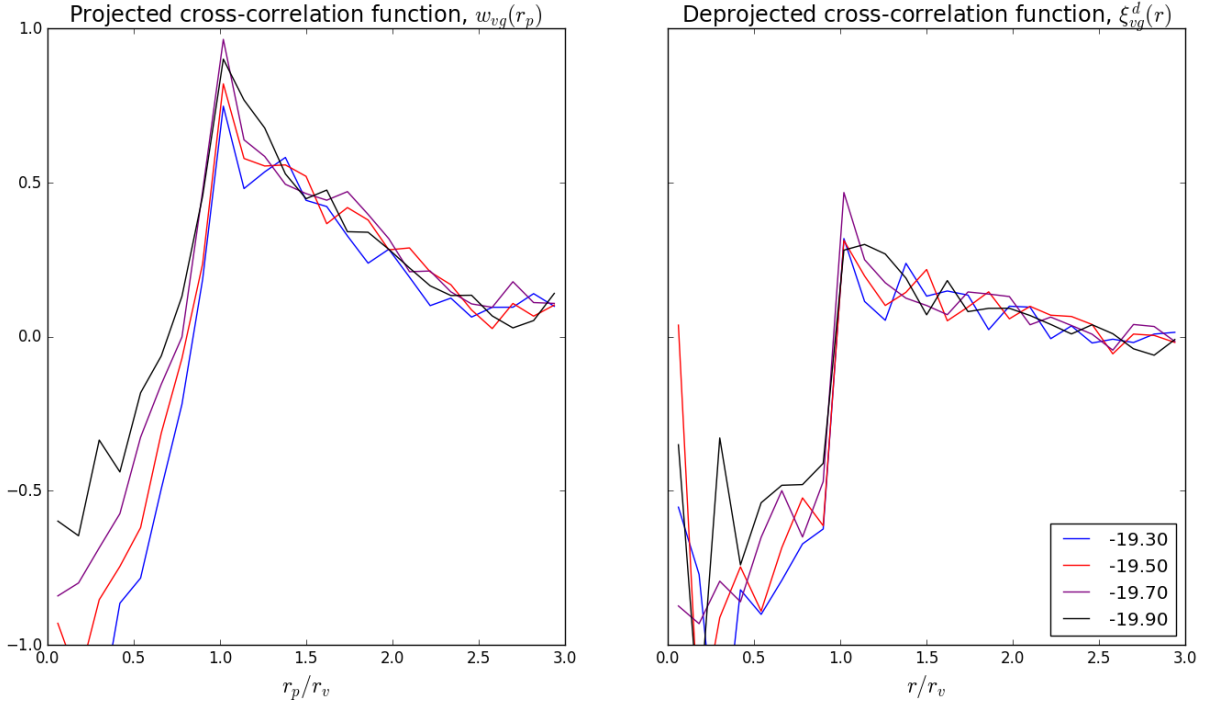
Fig. 10. Projected cross-correlation functions (*left hand panel*) and de-projected density profiles (*right hand panel*) for voids in VIPERS, found in volume-limited catalogues with different magnitude cuts. When a brighter magnitude cut is used to define the volume limited catalogue the voids found are less empty and thus the interior void profile changes.
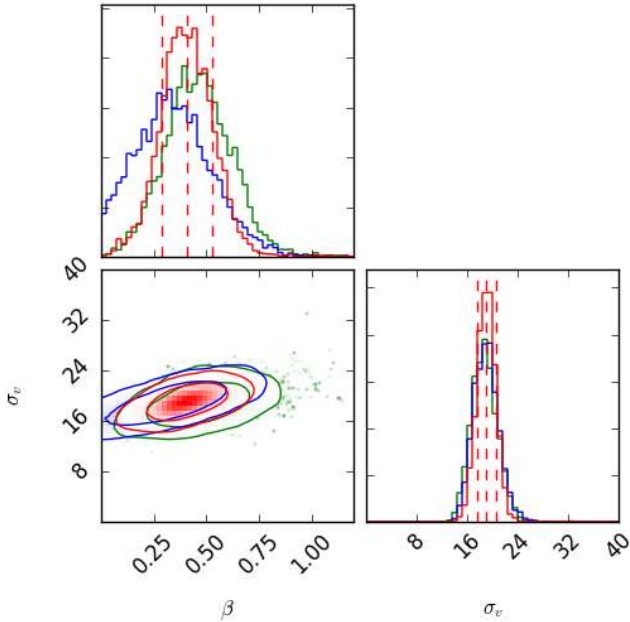

Fig. 11. MCMC contours for a two parameter RSD model fitted to VIPERS. The green contours indicate the fit to W4, the blue to W1, and the red contours are from the combination of the two fields. The dashed red lines represent the 16th, 50th and 84th percentiles.

where $R = 8 \, h^{-1}$ Mpc and

$$g(x) = \begin{cases} \frac{1}{2\pi}[3\pi - 9x + x^3] & \text{if } x \le 2 \\ \frac{1}{2\pi}\left[\frac{-x^4 + 11x^2 - 28}{\sqrt{x^2 - 4}} + x^3 - 9x + 6\sin^{-1}\left(\frac{2}{x}\right)\right] & \text{if } x > 2. \end{cases} \quad (36)$$

The projected correlation function is defined as

$$w_{\mathrm{p}}(r_{\mathrm{p}}) = 2 \int_{r_{\mathrm{p}}}^{\infty} \frac{r\,\xi(r)}{\sqrt{r^2 - r_{\mathrm{p}}^2}} \, \mathrm{d}r = 2 \int_{0}^{\infty} \xi\left(\sqrt{r_{\mathrm{p}}^2 + r_{\pi}^2}\right) \mathrm{d}r_{\pi}, \quad (37)$$

where r is the apparent co-moving separation of galaxy pairs, r_{π} is the line-of-sight separation, and r_{p} is their projected separation perpendicular to the line of sight. We measured $w_{\mathrm{p}}(r_{\mathrm{p}})$ by using the Landy-Szalay estimator to measure $\xi(r_{\mathrm{p}}, r_{\pi})$ of galaxies, and integrated it using Eq. (37). In practice, the limits of the integral in Eq. (37) are finite and determined by observational constraints. On scales $r < 1 \, h^{-1}$ Mpc the galaxy autocorrelation function is dominated by systematic effects, namely the TSR and SSR (see de la Torre et al. 2013). We could not measure scales $r_{\pi} \gg 100 \, h^{-1}$ Mpc due to the finite size of the survey. The limits of the integral were thus taken to be $1 \, h^{-1}$ Mpc $< r_{\pi} < 120 \, h^{-1}$ Mpc. This result was then integrated using Eq. (35) to obtain an estimate of $\sigma_8^{\mathrm{galaxies}}$.

The "linear" value of $\sigma_8^{\mathrm{galaxies}}$ could then be estimated by multiplying by the factor $\sigma_8^{\mathrm{linear}}/\sigma_8^{\mathrm{nonlinear}}$, which is the ratio of the linear and non-linear values for the σ_8 of dark matter, calculated from a CAMB power spectrum, respectively without and with a HALOFIT model for the non-linear part. The ratio $\sigma_8^{\mathrm{linear}}/\sigma_8^{\mathrm{nonlinear}}$ is fairly model-independent, and therefore the use of a fiducial power spectrum should not affect our result. However, using the ratio computed for dark matter to estimate the same ratio for galaxies implicitly assumes linear biasing.

We measured a mean value of $\sigma_8^{\mathrm{galaxies}} = 0.735 \pm 0.043$ in our mock catalogues, which is consistent with the estimate of the bias presented in Sect. 7.2. The value recovered from the data is $\sigma_8^{\mathrm{galaxies}} = 0.700$. Our estimate of $f\sigma_8$ is then $f\sigma_8 = 0.296^{+0.075}_{-0.078}$. Figure 12 shows this value compared to other measurements.
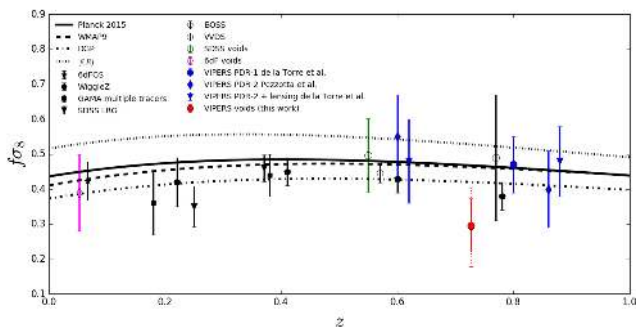
Fig. 12. Comparison to other estimates of the growth rate (Beutler et al. 2012; Blake et al. 2011, 2013; Samushia et al. 2012, 2014; Guzzo et al. 2008), error bars show 1σ errors. Of particular interest are the measurement using conventional galaxy clustering techniques on VIPERS PDR-1 (blue filled circle: de la Torre et al. 2013); the measurement using voids in SDSS (green open circle: Hamaus et al. 2016); and the measurement using voids in 6dF (magenta diamond: Achitouv & Blake 2017). The measurement presented in this work is the red point, the solid error bars on this point are those estimated from the mocks, and the dashed error bars are those estimated using MCMC.

9. Discussion and conclusion

Using the final data set of VIPERS we produced an updated void catalogue. We measured the anisotropic cross-correlation between the centres of voids in this catalogue and the full VIPERS galaxy sample. By de-projecting the anisotropic cross-correlation we are able to estimate the un-distorted density profile. We demonstrate, first using a toy model and then using mock galaxy catalogues, that by fitting a model which includes linear redshift space distortions to the cross-correlation we recover an estimate of the linear growth rate parameter β. Applying this to the combined data set of the two VIPERS fields we obtain a measurement of $\beta_{\mathrm{VIPERS}} = 0.423^{+0.104}_{-0.108}$. We convert this to a value for the linear growth rate of $f\sigma_8 = 0.296^{+0.075}_{-0.078}$.

There is no significant tension between our measurement and that obtained from a conventional analysis of the VIPERS data, although our measurement appears to be slightly lower. Our measurement is commensurate with other published results using more conventional methods.

The dominant source of uncertainty is cosmic variance. The usefulness of the void-galaxy cross-correlation function from VIPERS for constraining cosmology is limited by the size and geometry of the survey. Because our mock catalogues have a VIPERS-like geometry, we cannot investigate possible constraints from a larger contiguous region and are restricted to studying scenarios with VIPERS-like fields. It is likely that a larger contiguous survey would provide much tighter constraints.

Our algorithm rejects spheres when less than 80% of the volume falls within the survey. One of the results of this is that close to the borders of the survey voids can become fragmented, with large spheres being replaced by many smaller ones. Border effects are not unique to our algorithm; ZOBOV (ZOnes Bordering On Voidness) based void-finders also have problems describing voids that lie close to survey boundaries (Neyrinck 2008). A popular approach to dealing with this problem is to exclude voids that lie close to the borders from the analysis. However, the geometry of VIPERS makes it particularly susceptible to border effects. In Fig. 4, the signal from W4 appears noisier, by eye, than the signal from W1. It is worth pointing out that, being smaller, W4 will be more affected by border effects than W1. Almost all

voids intersect with at least one survey boundary, meaning that excluding voids which intersect with borders from the analysis would be unfeasible.

Our model for the redshift space distortions around voids, outlined in Sect. 4, assumes that the centres of empty spheres correspond to maxima in the gravitational potential field, in other words points from which galaxies are outflowing. Although our results clearly indicate a positive detection of outflows from voids, it may well not be the case that the centres of our spheres correspond to the centres of these outflows. Any random offset is likely to dilute the redshift space distortion signal and add to the uncertainty in the estimate of β. However, this is allowed for in mocks and we see no such effect.

If it is the case that the properties of galaxies in the void interiors are significantly different to those outside, then they will be biased with respect to the dark matter distribution in different ways. In this paper we assumed that the galaxy bias is strictly linear and scale-independent. A more thorough model for the velocity field should consider scale-dependent bias around voids (Neyrinck et al. 2014).

To date there are two other works to have attempted measuring β from the void-galaxy cross-correlation in data: they are Achitouv & Blake (2017) and Hamaus et al. (2016; green and magenta points of Fig. 12). These results were released whilst our analysis was being carried out.

There are several key differences between the work of Hamaus et al. (2016) and ours. In terms of methodology, instead of directly de-projecting the void density profile they assume a certain functional form for it and then marginalise over the parameters of their model. The Sloan Digital Sky Survey (SDSS) covers a much larger volume than VIPERS, thus Hamaus et al. (2016) have many more galaxy-void pairs from which to measure the cross-correlation. They also probe different scales to us. Their voids range in size from $24\,h^{-1}$ Mpc to $64\,h^{-1}$ Mpc. The largest void in our analysis has a radius of $20.8\,h^{-1}$ Mpc, smaller than their smallest void, whereas their largest void bin is comparable to the width of VIPERS. This could have an impact on the accuracy of our redshift space distortion model, because it is understood that velocity fields of smaller voids are less linear than those of larger ones. It can therefore be expected that a linear description of the velocity field around voids is a less good description for a survey such as VIPERS than for SDSS. However, any changes to the recovered growth rate from improved modelling are likely to remain within the current error bar.

Achitouv & Blake (2017) look at the void-galaxy cross-correlation in the 6dF survey. They take an un-distorted ξ_{vg} calibrated on dark matter simulations and fit it to the anisotropic cross-correlation. Their algorithm is able to select voids of a certain size, $\sim 20\,h^{-1}$ Mpc fitting a particular profile. Some of their voids overlap, whereas ours are defined not to. They exclude some bins on small scales to mask out non-linearities. The number of spectra measured in the 6dF survey is of the same order of magnitude as that measured by VIPERS.

Cai et al. (2016) present a method for measuring the linear growth rate β using the multipoles of the void-galaxy cross-correlation function. They then apply this method to simulations and demonstrate that given a volume of $3\,\mathrm{Gpc}^3\,h^{-3}$ they can recover β to within 10%. Their methodology has some similarities to ours. Firstly they define their voids using under-dense spheres, as do we. Secondly their approach does not require a model for the void density profile, because they are able to derive this from the multipoles. There are some differences in their redshift space distortion modelling. For example, for most of their analysis they ignore the velocity dispersion, σ_{v}, and correlations close to the

void centres. However, when they include σ_v and the void interiors they are able to reduce the uncertainty of β.

The precision of our measurement is consistent with the precision of Achitouv & Blake (2017) and is better than that of Hamaus et al. (2016), given the difference in survey volume. Although VIPERS may not provide the most accurate measurement of the growth rate of structure in low density environments, it provides a measurement at higher redshift than other current observations. Thus our results limit any gross deviations from Einstein gravity at high redshift.

In two parallel papers of this series the growth rate of structure is measured using more conventional techniques. Pezzotta et al. (2017) measure the growth rate by modelling the multipoles of the anisotropic autocorrelation in configuration space. They find $f\sigma_8 = 0.55 \pm 0.12$ and 0.40 ± 0.11 at $z = 0.6$ and 0.86 respectively (blue diamonds Fig. 12). de la Torre et al. (2016) combine RSD measurements from VIPERS with lensing data from the CFHTLenS survey over the same area of sky to constrain the growth rate of structure. They find $f\sigma_8 = 0.48 \pm 0.12$ and $f\sigma_8 = 0.48 \pm 0.10$ at $z = 0.6$ and 0.86 respectively (blue triangles Fig. 12). Our estimate is lower than those obtained from VIPERS in Pezzotta et al. (2017) and de la Torre et al. (2016). Estimating the growth rate from the void-galaxy cross-correlation function is clearly still in its infancy, with potential systematic errors not yet fully understood. Nevertheless, accounting for the different effective redshifts of the measurements, the different VIPERS values for the growth rate are consistent at the 1-sigma level.

References

Achitouv, I., & Blake, C. 2017, Phys. Rev. D, 95, 083502
Albrecht, A., Amendola, L., Bernstein, G., et al. 2009, ArXiv e-prints [arXiv:0901.0721]
Beutler, F., Blake, C., Colless, M., et al. 2012, MNRAS, 423, 3430
Blake, C., Brough, S., Colless, M., et al. 2011, MNRAS, 415, 2876
Blake, C., Baldry, I. K., Bland-Hawthorn, J., et al. 2013, MNRAS, 436, 3089
Bottini, D., Garilli, B., Maccagni, D., et al. 2004, A&A, submitted [arXiv:astro-ph/0409252]
Cai, Y.-C., Padilla, N., & Li, B. 2015, MNRAS, 451, 1036
Cai, Y.-C., Taylor, A., Peacock, J. A., & Padilla, N. 2016, MNRAS, 462, 2465
Chuang, C.-H., Kitaura, F.-S., Liang, Y., et al. 2017, Phys. Rev. D, 95, 063528
Clampitt, J., Cai, Y.-C., & Li, B. 2013, MNRAS, 431, 749
Cuillandre, J.-C. J., Withington, K., Hudelot, P., et al. 2012, in SPIE Conf. Ser., 8448, 0
Davis, M., & Peebles, P. J. E. 1983, ApJ, 267, 465
de la Torre, S., & Peacock, J. A. 2013, MNRAS, 435, 743
de la Torre, S., Guzzo, L., Peacock, J. A., et al. 2013, A&A, 557, A54
de la Torre, S., Jullo, E., Giocoli, C., et al. 2016, A&A, submitted [arXiv:1612.05647]
Dubinski, J., da Costa, L. N., Goldwirth, D. S., Lecar, M., & Piran, T. 1993, ApJ, 410, 458
Eisenstein, D. J. 2003, ApJ, 586, 718
Finelli, F., Garcia-Bellido, J., Kovacs, A., Paci, F., & Szapudi, I. 2016, MNRAS, 455, 1246
Foreman-Mackey, D., Hogg, D. W., Lang, D., & Goodman, J. 2013, PASP, 125, 306
Garilli, B., Guzzo, L., Scodeggio, M., et al. 2014, A&A, 562, A23
Goldberg, D. M., & Vogeley, M. S. 2004, ApJ, 605, 1
Guzzo, L., Pierleoni, M., Meneux, B., et al. 2008, Nature, 451, 541
Hamaus, N., Sutter, P. M., Lavaux, G., & Wandelt, B. D. 2014a, J. Cosmol. Astropart. Phys., 12, 13
Hamaus, N., Sutter, P. M., & Wandelt, B. D. 2014b, Phys. Rev. Lett., 112, 251302
Hamaus, N., Sutter, P. M., Lavaux, G., & Wandelt, B. D. 2015, J. Cosmol. Astropart. Phys., 11, 036
Hamaus, N., Pisani, A., Sutter, P. M., et al. 2016, Phys. Rev. Lett., 117, 091302
Hamilton, A. J. S. 1998, in The Evolving Universe, ed. D. Hamilton, Astrophys. Space Sci. Lib., 231, 185
Hartlap, J., Simon, P., & Schneider, P. 2007, A&A, 464, 399
Hoyle, F., Vogeley, M. S., & Pan, D. 2012, MNRAS, 426, 3041
Jennings, E., Li, Y., & Hu, W. 2013, MNRAS, 434, 2167
Kaiser, N. 1987, MNRAS, 227, 1
Kreckel, K., Platen, E., Aragón-Calvo, M. A., et al. 2012, AJ, 144, 16
Landy, S. D., & Szalay, A. S. 1993, ApJ, 412, 64
Lewis, A., & Bridle, S. 2002, Phys. Rev., D66, 103511
Linder, E. V. 2005, Phys. Rev. D, 72, 043529
Linder, E. V., & Cahn, R. N. 2007, Astropart. Phys., 28, 481
Micheletti, D., Iovino, A., Hawken, A. J., Granett, B. R., & VIPERS Team 2014, A&A, 570, A106
Nadathur, S., Hotchkiss, S., Diego, J. M., et al. 2015, MNRAS, 449, 3997
Neyrinck, M. C. 2008, MNRAS, 386, 2101
Neyrinck, M. C., Aragón-Calvo, M. A., Jeong, D., & Wang, X. 2014, MNRAS, 441, 646
Padilla, N. D., Ceccarelli, L., & Lambas, D. G. 2005, MNRAS, 363, 977
Patiri, S. G., Prada, F., Holtzman, J., Klypin, A., & Betancort-Rijo, J. 2006, MNRAS, 372, 1710
Paz, D., Lares, M., Ceccarelli, L., Padilla, N., & Lambas, D. G. 2013, MNRAS, 436, 3480
Peebles, P. J. E. 1980, The large-scale structure of the universe (Princeton University Press)
Percival, W. J., Ross, A. J., Sánchez, A. G., et al. 2014, MNRAS, 439, 2531
Pezzotta, A., de la Torre, S., Bel, J., et al. 2017, A&A, 604, A33
Pisani, A., Lavaux, G., Sutter, P. M., & Wandelt, B. D. 2014, MNRAS, 443, 3238
Platen, E., van de Weygaert, R., & Jones, B. J. T. 2007, MNRAS, 380, 551
Prada, F., Klypin, A. A., Cuesta, A. J., Betancort-Rijo, J. E., & Primack, J. 2012, MNRAS, 423, 3018
Ricciardelli, E., Cava, A., Varela, J., & Quilis, V. 2014, MNRAS, 445, 4045
Rojas, R. R., Vogeley, M. S., Hoyle, F., & Brinkmann, J. 2004, ApJ, 617, 50
Ross, N. P., da Ângela, J., Shanks, T., et al. 2007, MNRAS, 381, 573
Samushia, L., Percival, W. J., & Raccanelli, A. 2012, MNRAS, 420, 2102
Samushia, L., Reid, B. A., White, M., et al. 2014, MNRAS, 439, 3504
Sellentin, E., & Heavens, A. F. 2016, MNRAS, 456, L132
Sheth, R. K., & van de Weygaert, R. 2004, MNRAS, 350, 517
Sutter, P. M., Lavaux, G., Wandelt, B. D., & Weinberg, D. H. 2012, ApJ, 761, 44
Takahashi, R., Sato, M., Nishimichi, T., Taruya, A., & Oguri, M. 2012, ApJ, 761, 152
von Benda-Beckmann, A. M., & Mueller, V. 2007, ArXiv e-prints [arXiv:0710.2783]
Wang, L., & Steinhardt, P. J. 1998, ApJ, 508, 483
Zehavi, I., Eisenstein, D. J., Nichol, R. C., et al. 2005, ApJ, 621, 22
Zivick, P., Sutter, P. M., Wandelt, B. D., Li, B., & Lam, T. Y. 2015, MNRAS, 451, 4215

[1] INAF–Osservatorio Astronomico di Brera, via Brera 28, 20122 Milano, via E. Bianchi 46, 23807 Merate, Italy
e-mail: adam.hawken@brera.inaf.it

[2] Università degli Studi di Milano, via G. Celoria 16, 20130 Milano, Italy

[3] INAF – Istituto di Astrofisica Spaziale e Fisica Cosmica Milano, via Bassini 15, 20133 Milano, Italy

[4] Aix-Marseille Université, CNRS, LAM (Laboratoire d'Astrophysique de Marseille) UMR 7326, 13388 Marseille, France

[5] INAF–Osservatorio Astronomico di Torino, 10025 Pino Torinese, Italy

[6] Canada-France-Hawaii Telescope, 65–1238 Mamalahoa Highway, Kamuela, HI 96743, USA

[7] Aix-Marseille Université, CNRS, CPT, UMR 7332, 13288 Marseille, France

[8] INAF–Osservatorio Astronomico di Bologna, via Ranzani 1, 40127 Bologna, Italy

[9] Dipartimento di Matematica e Fisica, Università degli Studi Roma Tre, via della Vasca Navale 84, 00146 Roma, Italy

[10] Institute of Cosmology and Gravitation, Dennis Sciama Building, University of Portsmouth, Burnaby Road, Portsmouth, PO1 3FX, UK

[11] INAF–Osservatorio Astronomico di Trieste, via G. B. Tiepolo 11, 34143 Trieste, Italy

[12] Institute for Astronomy, University of Edinburgh, Royal Observatory, Blackford Hill, Edinburgh EH9 3HJ, UK

[13] Institute of Physics, Jan Kochanowski University, ul. Swietokrzyska 15, 25-406 Kielce, Poland

[14] Department of Particle and Astrophysical Science, Nagoya University, Furo-cho, Chikusa-ku, 464-8602 Nagoya, Japan

[15] Dipartimento di Fisica e Astronomia, Alma Mater Studiorum Università di Bologna, viale Berti Pichat 6/2, 40127 Bologna, Italy

[16] INFN, Sezione di Bologna, viale Berti Pichat 6/2, 40127 Bologna, Italy

[17] Laboratoire Lagrange, UMR 7293, Université de Nice Sophia Antipolis, CNRS, Observatoire de la Côte d'Azur, 06300 Nice, France

[18] Astronomical Observatory of the Jagiellonian University, Orla 171, 30-001 Cracow, Poland

[19] National Centre for Nuclear Research, ul. Hoza 69, 00-681 Warszawa, Poland

[20] INAF–Istituto di Astrofisica Spaziale e Fisica Cosmica Bologna, via Gobetti 101, 40129 Bologna, Italy

[21] INAF–Istituto di Radioastronomia, via Gobetti 101, 40129 Bologna, Italy

[22] INFN, Sezione di Roma Tre, via della Vasca Navale 84, 00146 Roma, Italy

[23] INAF–Osservatorio Astronomico di Roma, via Frascati 33, 00040 Monte Porzio Catone (RM), Italy